European Journal of Pharmaceutics and Biopharmaceutics 201 (2024) 114368

Contents lists available at ScienceDirect

European Journal of Pharmaceutics and Biopharmaceutics

journal homepage: www.elsevier.com/locate/ejpb

Research paper

Real-time release testing of *in vitro* dissolution and blend uniformity in a continuous powder blending process by NIR spectroscopy and machine vision

Lilla Alexandra Mészáros, Martin Gyürkés, Emese Varga, Kornélia Tacsi, Barbara Honti, Enikő Borbás, Attila Farkas, Zsombor Kristóf Nagy, Brigitta Nagy *

Department of Organic Chemistry and Technology, Faculty of Chemical Technology and Biotechnology, Budapest University of Technology and Economics, Műegyetem rkp. 3., H-1111 Budapest, Hungary

ARTICLE INFO

Keywords:
Dissolution prediction
Continuous blending
Process analytical technology
Machine vision
Real-time release testing
End-to-end manufacturing

ABSTRACT

Continuous manufacturing is gaining increasing interest in the pharmaceutical industry, also requiring real-time and non-destructive quality monitoring. Multiple studies have already addressed the possibility of surrogate *in vitro* dissolution testing, but the utilization has rarely been demonstrated in real-time. Therefore, in this work, the in-line applicability of an artificial intelligence-based dissolution surrogate model is developed the first time. NIR spectroscopy-based partial least squares regression and artificial neural networks were developed and tested in-line and at-line to assess the blend uniformity and dissolution of encapsulated acetylsalicylic acid (ASA) – microcrystalline cellulose (MCC) powder blends in a continuous blending process. The studied blend is related to a previously published end-to-end manufacturing line, where the varying size of the ASA crystals obtained from a continuous crystallization significantly affected the dissolution of the final product. The in-line monitoring was suitable for detecting the variations in the ASA content and dissolution caused by the feeding of ASA with different particle sizes, and the at-line predictions agreed well with the measured validation dissolution curves ($f_2 = 80.5$). The results were further validated using machine vision-based particle size analysis. Consequently, this work could contribute to the advancement of RTRT in continuous end-to-end processes.

1. Introduction

In recent years, an extensive transformation of pharmaceutical manufacturing has been initiated, aiming for more flexible and efficient research and development, production, and quality control. From the technological perspective, it manifests in introducing continuous manufacturing steps [1] or even integrated, end-to-end continuous production [2]. From the quality point of view, the risk- and knowledge-based manufacturing initiated by the Quality by Design (QbD) concept, the real-time monitoring by Process Analytical Technology (PAT) Food and Drug Administration [3], and the potential of real-time release testing (RTRT) Agency [4] gain increasing interest. Although these concepts also apply to batch processes, they became indispensable for continuous production to truly benefit from operational flexibility [5,6]. The growing interest in continuous manufacturing and advanced quality control by QbD, PAT, and RTRT is well demonstrated by the vast number of publications from both the academia and industry, which are extensively reviewed in [6,7].

Powder blending is a crucial unit operation of downstream processing of final solid dosage forms, *e.g.*, tablets and capsules, to obtain homogeneous mixtures of components in the proper constitution. While in the case of batch blending, it is generally sufficient to analyze the endpoint of the mixing, the continuous operation entails the need to monitor the quality of the powder stream in-line [7]. Several studies have already dealt with the analysis of the critical quality attributes (CQAs) of continuous blending, *i.e.*, concentration, blend uniformity (BU), and the consequent content uniformity (CU) of the final product (usually tablets) [6,8]. For instance, the effect of different measurement setups of in-line NIR spectroscopic measurement on the BU results has been demonstrated [9], as well as the relationship of the BU and the tablet CU has been studied [9–11]. NIR spectroscopy has also been applied in the development of residence time distribution (RTD) model of the blending process [12], and feedback control of blend concentration has been achieved by applying in-line NIR [13], Raman

* Corresponding author.
E-mail address: nagy.brigitta@vbk.bme.hu (B. Nagy).

https://doi.org/10.1016/j.ejpb.2024.114368
Received 6 April 2024; Received in revised form 22 May 2024; Accepted 13 June 2024
Available online 14 June 2024

spectroscopy [14], as well machine vision [15].

The particle size of the blends can also account for a critical material attribute (CMA), such as in further feedability [16] or in the occurrence of segregation [17], which can affect the CU or even the *in vitro* dissolution of the final products. In [18], the authors have demonstrated that continuous blending decreases the risk of segregation and increases the blend homogeneity compared to the batch operation. Several studies have already demonstrated the applicability of NIR spectroscopy to quantify particle size differences in powder samples, which is reviewed in detail *e.g.*, in [19–21]. Several theories have attempted to describe the relationship between the NIR spectra and the particle size, but it still remained a complex field of study. It has been also shown that common preprocessing methods cannot entirely eliminate this effect [20,21]. Barajas *et al.* concluded that NIR spectroscopy could be used to detect post-blending segregation of flowing powder, not only due to the concentration change during the segregation but thanks to the particle size information carried in the NIR spectra [22].

A direct approach for detecting in-process particle size variations is the application of particle size measurement tools. Several measurement techniques exist for quantifying particle size distribution (PSD) in-line. Apart from the commonly used laser diffraction, there are a few alternatives within the field of machine vision or imaging technologies. These techniques utilize advanced image processing or artificial intelligence [23,24] and are gaining increasing interest in the pharmaceutical industry [23] due to their cost-efficiency, speed, non-invasiveness, and non-destructive nature [25]. Imaging techniques have the capability to analyze challenging samples that have a very diverse range or limited representation of particle sizes. They can serve as at-line, non-destructive techniques, similar to a microscopic particle size measurement. Nevertheless, when compared to a microscopic measurement, the developed system offers high-resolution images, easy accessibility in a cost-effective manner. The potency of novel technologies such as photometric stereo imaging, Eyecon®, and spatial filtering velocimetry were also compared, and the dissimilarities were explained based on their working principles [24]. Recently, Ficzere *et al.* utilized an AI-based machine vision system to evaluate the PSD of acetylsalicylic acid and calcium hydrogen phosphate, which involved the detection of particles exceeding 100 μm in size [26]. Madarász *et al.* also employed AI-based imaging techniques with an endoscope to perform in-line determination of particle size for sodium-chloride crystals ranging from 200-1000 μm [27].

In vitro dissolution is one of the most critical CQAs of the solid dosage forms, which is used to show bioequivalence as well as consistent quality by characterizing the inter- and intra-batch variability. The *in vitro* dissolution curves are affected by several CMAs and critical process parameters (CPPs) from different processing units and, therefore, can serve as a fingerprint of the whole manufacturing [28]. Several studies have already addressed the challenge of developing RTRT alternatives of dissolution, both for immediate- and extended-release products, although the immediate-release is more prevalent in regulatory submissions [28,29]. In these works, the CMAs and CPPs are first identified, then these factors are monitored by appropriate PAT measurement or process data collection. For example, NIR [30–33] and Raman spectroscopy [30,34] have been already successfully applied to dissolution surrogate modeling. Finally, mathematical modeling is carried out to establish the connection between the collected data and the *in vitro* dissolution curves, for which machine learning and artificial intelligence are gaining increasing interest [28], but mechanistic/white-box modeling is also a possibility [35,36]. Despite the numerous successful proof-of-concept studies, the real-time utilization of surrogate dissolution modeling has rarely been demonstrated. In [37], real-time NIR measurements performed within a pan coater were used to predict the dissolution of the final product, *i.e.*, a controlled-release tablet containing a functional coat. Su *et al.* [38] demonstrated the in-line application of a model-predictive dissolution prediction approach in an end-to-end extrusion-molding-coating manufacturing line. In their work, a mechanistic model was developed to account for the swelling and eroding of the immediate-release tablet, which was applied to monitor the variation of the dissolution caused by the changing mass fraction of the active pharmaceutical ingredient (API) measured by in-line NIR.

This work aims to elaborate on the in-line applicability of *in vitro* dissolution surrogate modeling by PAT tools. NIR spectroscopy-based partial least squares regression (PLS) and artificial neural network (ANN) models were developed and applied both in-line and at-line to simultaneously assess the blend uniformity and *in vitro* dissolution of encapsulated powder blends produced in a continuous blending process. To the best of the authors' knowledge, this is the first published in-line, real-time dissolution monitoring based on artificial neural networks (ANNs). The studied model system, *i.e.*, acetylsalicylic acid (ASA) – microcrystalline cellulose (MCC) blend, is the same as used for the development of an end-to-end continuous manufacturing line in our previous works [12,36,39,40], where the ASA particle size was found to be affected by the continuous crystallization conditions of the flow reaction [40], and influencing the *in vitro* dissolution of the final product. As the particle size information in the NIR spectra can be carried in a relatively weak signal, it was also critically important to validate the particle size determination using an orthogonal particle size measurement technique. For this purpose, the application of an at-line machine vision technique was selected, which can provide a cost-effective, non-destructive, and high-resolution approach for particle size analysis. The comparison of the two techniques highlighted the validity of ANN model, as well as the potential of the machine vision approach for at-line analysis, which could be further developed into in-line PAT technique with suitable sampling interface and data analysis technique. Consequently, this work could contribute to the advancement of RTRT in continuous end-to-end processes.

Table 1
Off-line calibration samples used for content and dissolution model development. The samples filled into capsules are indicated in bold.

Included ASA sieve fraction	ASA concentration [% w/w]
Unsieved	5, 10, 15, 20, 30, 40, **100**
< 63 μm	5, 15, 17.5, 20, 25, **100**
63–100 μm	22.5, **100**
100–150 μm	15, 17.5, 25, **100**
150–200 μm	15, 22.5, **100**
300–500 μm	5, 15, 20, 22.5, 25, **100**
50 % (63–100 μm) + 50 % (100–150 μm)	**20**
50 % (150–200 μm) + 50 % (300–500 μm)	**20**
MCC	0

2. Materials and methods

2.1. Materials

Acetylsalicylic acid (ASA) was used as a model drug, purchased from Sigma Aldrich (Germany), and microcrystalline cellulose (MCC, Vivapur® 200) was used as an excipient (JRS Pharma, USA). For dissolution testing purposes, concentrated hydrochloric acid solution was purchased from Merck Ltd. (Germany).

2.2. Sample preparation and experimental setup

As a model formulation, 150 mg ASA – MCC physical powder blends filled into hard gelatin capsules were studied with a nominal ASA content planned for 20 % w/w. In our previous studies [36,40], it was demonstrated that the PSD of the ASA critically affects its dissolution. In the preliminary phase of this work, it was studied if the API processing using a twin-screw blender or the addition of the MCC to the ASA impacts the dissolution (*e.g.*, due to agglomeration or breakage). The same dissolution curves were obtained irrespective of the MCC content and the blending method; therefore, the ASA PSD was identified as the only

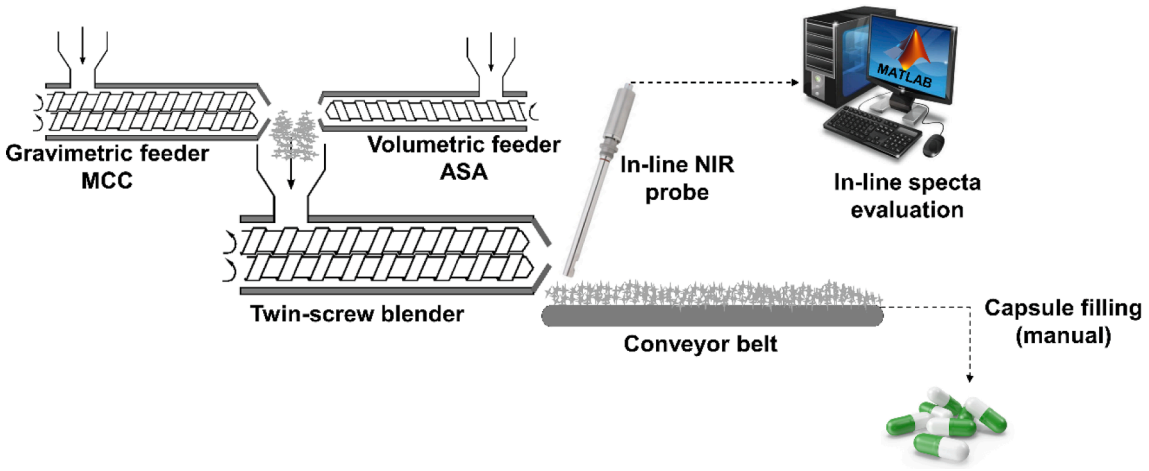

Fig. 1. Experimental setup of the continuous blending process.

critical parameter affecting the *in vitro* dissolution of the capsules. Consequently, we aimed to develop an RTRT method to determine the PSD-dependent dissolution and the ASA content of continuously produced powder blends simultaneously.

The raw material ASA was sieved using a CISA BA 200 N (Barcelona, Spain) apparatus with an amplitude of 2 mm. The process was run for a sufficiently long time (approx. 20 min) to reach constant mass fractions, *i.e.*, all particles had the opportunity to pass. The sieve fractions of < 63, 63–100, 100–150, 150–200, and 300–500 μm were collected. A total of 30 calibration powder blends were prepared with changing ASA PSD and content as detailed in Table 1. 5 g powder blends were prepared manually by weighing the appropriate amount of the ASA and excipient using an analytical balance and blending the components by thoroughly shaking the plastic container for 2 min. All the blends were further analyzed in powder form, and from selected samples (bold in Table 1), 3 hard gelatin capsules were manually filled with 150 mg powder for dissolution testing.

A continuous powder blending experiment was performed to test the performance of the off-line developed content and dissolution prediction methods. The experimental setup (see Fig. 1) consisted of a twin-screw FEEDMASTER LW–20–300 loss-in weight feeder (Dunaprecíziós Ltd., Dunakeszi, Hungary), which was used to feed the excipient, and a single-screw volumetric feeder (FPS Pharma, Fiorenzuola d'Arda, Italy) for the ASA feeding. The ASA feeder has smaller capacity which suited the lower ASA feed rates and equipped with the possibility of PID control by an in-house developed interface. The feeders were connected to a TS16 QuickExtruder® (Quick 2000 Ltd, Hungary) twin-screw multi-purpose equipment with a 16 mm (25 L/D ratio) screw diameter, which was used for continuous blending, but the equipment is also applicable for wet and melt granulation in case the die of the extruder is removed. The blending was operated with an approx. 0.3 kg/h mass flow rate, the corresponding feeding rates of the feeders were calibrated at the beginning of the experiment to achieve a 20 % w/w ASA content. Although we targeted the 20 % w/w content for the model formulation, no control of the feed rates was implemented in this study, which can cause deviations from this value. Furthermore, during the continuous operation, the feed rate was deliberately changed to analyze if the developed PAT method could effectively detect deviations. After the blender, the material was discharged into a conveyor belt.

The NIR spectra of the blend were measured every 5 s by a Bruker MPA Multi-Purpose NIR spectroscope coupled with an in-line Solvias fiberopic probe mounted over the conveyor belt near the blender's discharging point. The NIR measurement method is further detailed in Section 2.3.1. The spectrum collection time was 1 s, the corresponding analyzed sample size in the moving conveyor belt can be calculated using the following equation [14]:

$$Sample\ size[mg] = \left[\frac{d_{spot}^2\pi}{4} + d_{spot}tv\right]c\rho_t \quad (1)$$

where d_{spot} refers to the diameter of the probe (in this case 3 mm), t is the spectrum accumulation time (here 1 s), v is the conveyor belt velocity (approximately 7–8 mm/s), c refers to the thickness of the powder analyzed by the probe (approximated to 4 mm) and ρ_t is the bulk density of the freely settled powder, for which the bulk density of Vivapur 200 was accounted (0.37 g/ml). This results in approx. 40–45 mg powder analyzed during the 1 s spectrum collection. Consequently, to match the analyzed sample size with the NIR probe to the target dosage, an approx. 5 s spectral collection would be needed, which could be adjusted in future works. In-house developed Matlab interface and scripts were used to import the real-time collected spectra into Matlab and quantify the ASA concentration using the off-line developed PLS model (see Section 3.2). The interface also has the capability of feedback control [13,14]; however, no control was used in this experiment.

The blending experiment was operated for 30 min. The PSD of the fed ASA was deliberately changed during this time to model a potential segregation problem or varying raw material source in a blending/feeding operation. The ASA sieve fractions were fed as follows: at the beginning of the experiment, unsieved ASA was used, and then from the 3rd minute, the 300–500 μm sieve fraction was fed. In the approx. 16th minute, the feeder was refilled with the < 63 μm sieve fraction, followed by the 300–500 μm fraction from the 20th minute, and the experiment was finished using the unsieved fraction from the 25th minute. During the experiment, a total of 19 samples named *C1- C19* (approx. 1–2 g per sample) were taken from a narrow cross-section of the conveyor belt right after the location of the NIR measurement. The sampled powders were measured at-line by NIR spectroscopy and machine vision, manually filled into capsules (150 mg powder), and dissolution tests were performed on six randomly selected capsules, which were used for validation purposes (named *Valid C1, C3, C8, C10, C12, C14*).

As a conclusion of this section, the different samples and experiments used in this work are summarized in the following. A total of 30 calibration samples were prepared off-line, by changing the ASA particle size and content. Then, a continuous blending experiment was conducted, which was continuously monitored by NIR spectroscopy (in-line spectra), while 19 samples for at-line analysis (NIR and machine vision) were also taken (*C1- C19*). From these, six random samples (*Valid C1, C3, C8, C10, C12, C14*) were used for validation, *i.e.*, their *in vitro* dissolution was measured by the conventional dissolution technique.

2.3. Analytical methods

2.3.1. NIR spectroscopy

NIR spectra were recorded using a Bruker MPA Multi-Purpose FT-NIR Analyzer (Bruker Optik GmbH, Germany) coupled with the OPUS 7.5 software (Bruker Optik GmbH, Germany). The spectra collection was performed using a Solvias fiberoptic probe in reflection mode, a high-intensity Tungsten NIR source, and a PbS detector. The spectra were collected in the 12500–4000 cm^{-1} spectral range with a resolution of 8 cm^{-1}, using 4 scans per spectrum, double-sided, forward–backward acquisition, and 10 kHz scanner velocity. In this way, the collection of one spectrum takes approx. 1 s. The calibration powder samples, and the 19 samples collected during the continuous experiments were measured at-line, *i.e.*, the probe was placed on the surface of the powders. For this, approx. 1–5 g of powder was placed in an open plastic container (the amount of powder was not controlled strictly to ensure variability for the calibration models). In this way, 10 repeated measurements were performed by shaking the powder samples between measurements and placing the probe in different spots of the sample. During the continuous experiment, the NIR probe was mounted over the moving blend, and spectra were collected every 5 s.

2.3.2. Image acquisition layout

The PSDs of the raw materials, calibration, and validation were determined using a machine vision system that relies on VIS imaging to validate the results of the models developed using NIR spectroscopy. The authors have previously published the in-house built layout for image acquisition [41]. A Canon 650D DSLR (Canon, Japan) camera was utilized with a Canon EFS 18–55 mm lens (Canon, Japan), which was mounted using a reversing ring. The light source was a ring light equipped with three rows of white LEDs. The system calibration was performed using the QPCard 101 v3 millimeter reference scale (Argraph Corp., NJ, USA). A resolution of 2.4 μm per pixel was successfully attained. The USB 3.0 interface facilitated the connection between the laptop and the camera. The dimensions of the acquired images were 3456 by 5184 pixels. The samples of the powders were carefully laid on a black background, taking care to prevent the overlapping of the particles. In one run a total of 10 images were acquired per powder sample. The captured regions on the images contain different quantities of particles depending on their respective sizes. The acquired images contained an average of 22 000 examined particles per sample; therefore, it is deemed to be representative of the sample.

2.3.3. In vitro dissolution testing

The *in vitro* dissolution testing of the capsules was performed using a Hanson SR8-Plus (Hanson Research, USA) dissolution tester, coupled with a Hanson Autoplus Maximizer 8 automatic pump (Hanson Research, USA) and an Agilent 8453 UV–VIS spectrophotometer (Hewlett-Packard, USA), which enabled automated sampling and concentration measurement. The Ph.Eur./USP paddle method was in sink condition. The dissolution medium of 900 mL of 0.1 N HCl solution was used, which is a common medium for immediate-release formulations of high solubility drug substances [42]. The medium was stirred at 100 rpm, and the temperature was kept at a constant 37 ± 0.5 °C during the test. The capsules were placed into spiral capsule sinkers to prevent floating. The dissolution was followed for 120 min, sampling at 2, 5, 10, 15, 20, 25, 30, 35, 40 min and every 10 min afterward. A univariate calibration curve using the UV absorbance peak at 228 nm was fitted with $R^2 = 0.99611$ before the dissolution testing to determine the dissolved ASA concentration. All the measured dissolution curves were normalized to 0–100 % dissolution for the better comparability of samples with different drug content, 100 % meaning the dissolved concentration at the 120^{th} min of the given capsule. The real, not-normalized ASA content of the validation samples was derived from the 120 min measurement time based on the calibration curve.

2.4. Mathematical modeling

Data analysis was performed using MATLAB 9.12. (MathWorks, USA) coupled with Deep Learning Toolbox 14.4., Statistics and Machine Learning Toolbox 12.3, and the PLS Toolbox 9.1. (Eigenvector Research, USA).

2.4.1. Principal component analysis

Principal component analysis (PCA) was performed on the NIR spectra to qualitatively analyze the information content of the calibration dataset and to reduce the spectral dimension before the ANN training. During PCA, the $n \times \lambda$ sized original dataset (where n and λ correspond to the number of the spectra and spectral variables, *i.e.*, wavenumbers, respectively) undergoes a coordinate transformation, aiming to incorporate the maximum variance of the dataset into the first few new variables (principal components, PCs) while keeping the PCs orthogonal to each other.

Preprocessing methods were applied on the spectra to enhance the information that were the most important for the modeling, while eliminating the noise/not required information. After initial screening of spectral preprocessing methods, the PCA model was built using the 9100–4400 cm^{-1} spectral range, preprocessed by standard normal variate (SNV), Savitzky-Golay smoothing and first derivative (second order polynomial, window size of 17 and weighted tails) and mean centering, as this setting resulted in the most distinct grouping of the scores corresponding to the API particle size and content.

2.4.2. Partial least squares regression

A partial least squares (PLS) regression model was built to quantify the ASA content in the ASA-MCC blends. Similar to PCA, PLS performs a coordinate transformation on the original spectral dataset, but the new variables (latent variables, LV) aim to maximize the covariance between the dependent variable (in this case, concentration). In this work, the NIR spectra were preprocessed before PLS regression the same way as for the PCA model (*i.e.*, SNV, Savitzky-Golay smoothing and first derivative, and mean centering). The genetic algorithm variable selection method was used as implemented in the PLS Toolbox (window width: 10, population size: 128, mutation rate: 0.005, double crossover, max. generations: 100) to choose the best combination of spectral ranges through a global optimization process. Cross-validation was performed using random sample subsetting with 7 splits to assess the model performance during the model optimization and selecting the number of the applied LVs. The models were characterized using the determination coefficient (R^2) and root mean square error of calibration (R^2_C, RMSEC), cross-validation (R^2_{CV}, RMSECV), and prediction (R^2_P, RMSEP).

2.4.3. Vis-imaging-based evaluation of the particle size

VIS-imaging-based machine vision was used to determine the PSD of the calibration and the 19 at-line samples from the continuous experiments. The image processing and analysis algorithm was implemented in the Matlab R2020a environment (Mathworks, USA). The imported images were preprocessed by conversion to grayscale as part of the initial step. First, a contrast enhancement was performed, followed by the binarization of the images. In some instances, the ASA crystals displayed transparent areas, resolved by applying a filling step based on pixel connectivity. In the binarization process, the background was denoted by zeros, while ones represented the particles. By employing the coordinates of the bounding boxes of the particles, that came into contact with the boundaries of the binary images were successfully eliminated. The application of these steps allowed the evaluation of small and non-aggregated particles. By utilizing the binary images, thresholds were determined in the last step for large particles, incorporating both size and color thresholds on the B channel. This approach allowed the visualization and elimination of the aleatory occurring large aggregates from the images. The area-equivalent diameters were computed in pixels for each particle based on the obtained images and subsequently con-

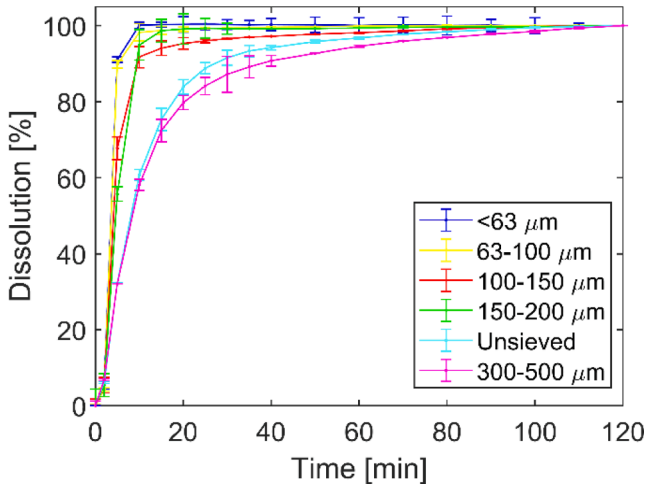

Fig. 2. Dissolution of the different ASA particle fractions.

verted to microns. The volume-based distribution was calculated by multiplying the number-based density function with x^3, where x refers to the mean values of the particle size channels, which is the common technique for converting number-based PSDs to volume-based. The distributions were normalized to unit maximum. Furthermore, statistical parameters from the distributions (Dv10, Dv50, Dv90, D10, D32, D43) were calculated. Dv10, Dv50 and Dv90 are the 10^{th}, 50^{th} and 90^{th} percentile of the cumulative volume distribution. D10, D32 and D43 refer to the number-weighted, area-weighted (Sauter-) and volume-weighed (De Brouckere-) mean diameter, respectively. The D10, D32 and D43 values were calculated with the equation of

$$\frac{\sum_i^n D_i^a v_i}{\sum_i^n D_i^{a-1} v_i} \quad (2)$$

, where D_i refers to the geometric mean of the i^{th} size channel, v_i the percent along the total n channels of the discretized distribution (in this study, $n = 100$ was applied). a is 1, 3 and 4 for D10, D32 and D43, respectively.

2.4.4. Artificial neural networks

Feedforward fully connected artificial neural networks (ANNs) were built to determine the *in vitro* dissolution of the capsules using different combinations of the information derived from the NIR spectra and PSD measurements. The ANNs consisted of 3 layers: an input layer that accepted the input features, a hidden layer with tangent hyperbolic activation function, and an output layer with linear activation function, which outputs the dissolution at each timepoint via a separate neuron (*i.e.*, a total of 18 output neurons were used). The number of neurons within the hidden layer was optimized by systematically building ANNs, varying the neuron numbers between 1 and 10 and performing 50 repetitions at each number. The model performance was compared using the f_1 difference and f_2 similarity factors [43] between the target and calculated dissolution curves. The f_1 and f_2 parameters range between 0 and 100; the lower f_1 and higher f_2 values indicate better performance. During model building, the calibration dataset was randomly divided into training, validation, and test sets in 80, 10, and 10 % ratios, respectively, while the continuous samples were used as independent test samples. The ANNs were trained using the Bayesian regularization training algorithm and the mean squared error (MSE) as a cost function. A bootstrap resampling with 500 resampling and subsequent ANN training was implemented with the optimized hidden layer size to account for the stochastic nature of the ANN training. In this way, an ensemble of the 500 ANN submodels is regarded as the 'ANN model', and the confidence interval of the model could be obtained as the 2.5 and 97.5 percentiles of the 500 models.

3. Results and discussion

3.1. Qualitative analysis of the calibration data

The *in vitro* dissolution curves of the capsules including only the pure ASA sieve fractions are illustrated in Fig. 2, which shows a significant variation in the dissolution corresponding to the changing particle size. In preliminary work, capsules with different ASA-MCC ratios were also measured, and it was observed that the presence of the excipient does not affect the dissolution curve (normalized to 100 % API content). The measured variation can be deemed critical considering an immediate-release dissolution criterium where 85 % dissolution in 15 min in 0.1 N HCl is expected for a BCS I drug (such as ASA) [44]. For example, in this case, the raw material (*i.e.*, unsieved) ASA and the 300–500 μm sieve fraction could not be counted as immediate-release. The variation in the raw material can be especially relevant when the risk of segregation is high or when the blending is performed in an end-to-end continuous manufacturing line when the crystallization step might provide the raw material with varying PSD.

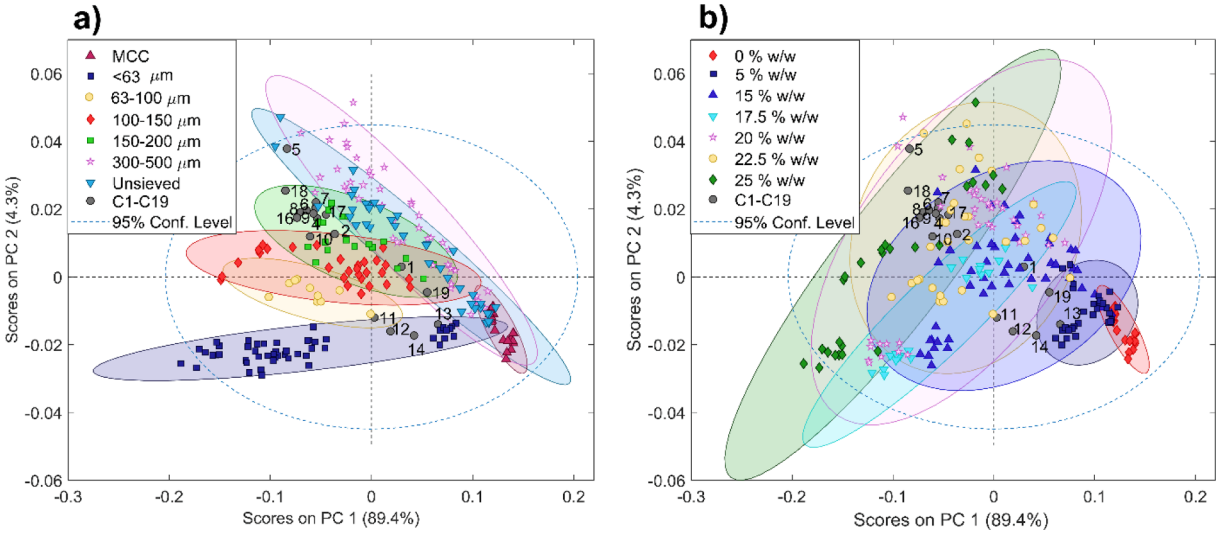

Fig. 3. PC 1- PC 2 score plot of the PCA model. The ellipses are associated with the 95% confidence interval of the given particle size groups. (The numbers of the grey circles refer to the number of the continuous samples, named C1-C19).

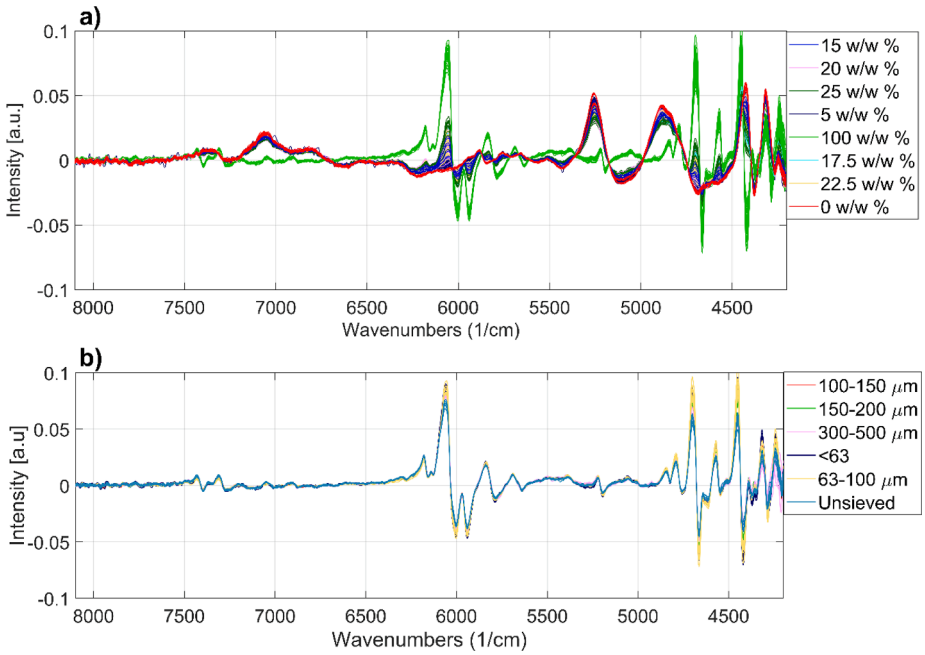

Fig. 4. Preprocessed NIR spectra (SNV, 1st derivative) of the calibration samples a) colored corresponding to the ASA concentration b) colored corresponding to the ASA particle size. In b) only the pure ASA samples are illustrated.

The PCA model was built by using the NIR spectra of the calibration samples to identify the main effects associated with the spectral variance. The preprocessing method was carefully selected during the initial screening of the preprocessing strategies. The screening resulted in the selection of SNV and Savitzky-Golay smoothing and first derivative, as this setting resulted in the most distinct grouping corresponding to the particle size and API content in the PCA model. The first three principal components (PCs) explained 94.9 % of the total spectral variance in the dataset, PC 1, PC 2, and PC 3 corresponding to 89.4, 4.3 and 1.2 % variance, respectively. As for PC 3, the incorporated 1.2 % variance could not be assigned to physical meaning based on the score and loading plots. Fig. 3 depicts the PC 1 – PC 2 score plot. In Fig. 3/a) different markers of the samples indicate the incorporated ASA particle size, in Fig. 3/b) the same score plot is color as per the ASA content, and the ellipses are associated with the 95 % confidence intervals of the given groups. Fig. 3/a) clearly shows the clustering of the calibration samples based on the particle size: the particle size mainly increasing diagonally from the lower left corner to the direction of the upper right corner of the score plot. Overlapping of the clusters is visible mainly for the unsieved and the 300–500 μm sieve fraction, which corresponds to the similar dissolution curves seen in Fig. 2, and the fact that the unsieved material contains a lot of particles sized between 300–500 μm. In Fig. 3/b, the change through the API content is depicted, which shows an orthogonal clustering compared to the particle size clusters, the API content increasing from the lower right corner in the direction to the upper left corner of the plot. It is also noticeable that the 15, 17.5, 20, 22.5 % w/w clusters are highly overlapping, which could be associated with inaccurate API content for certain samples. However, the PLS regression could be still improved with applying appropriate variable selection, as well as the PLS regression creates the latent variables by accounting for the covariance between the spectra and the concentration, which can improve the quantification. In Fig. 3, the PC scores of the continuous experiments (*C1-C19*) are also depicted, which is further discussed in Section 3.3.

The NIR spectra of the calibration set, preprocessed by SNV and first derivative, are illustrated in Fig. 4. In Fig. 4/a), the effect of the ASA concentration on the peak intensities is clearly visible. It was also observed that the ASA particle size differences manifest as slight intensity differences superposed on the spectrum of ASA. This is illustrated in Fig. 4/b), where only the pure ASA samples are depicted for better visibility. Smaller particle sizes caused an increase in the intensity, which is best visible in more intensive peaks. The effect of the particle size on the spectra was not eliminated by preprocessing, which have been already reported in several publications, and associated with the complex nature of the scattering effect [19–21]. The appropriate preprocessing method could even enhance this effect as other physical effects, such as the random variation in the intensity due to the variation of the sample thickness is eliminated. These observations indicate that the NIR spectra can be used to simultaneously characterize the API content and particle size-dependent dissolution of the capsules.

3.2. Quantitative NIR models for content and dissolution determination

A PLS model was built in the 0–40 % w/w concentration range using the NIR spectra to determine the ASA concentration in the ASA-MCC blends. The reference ASA concentration was determined based on the weights (measured using an analytical balance) of the materials during sample preparation. The calibration samples were not removed from their sample container for the NIR measurements, therefore the concentrations derived from the weighted values were deemed to be accurate for calibration purposes. Furthermore, 10 spectra were collected from each sample (shaking the samples and placing the probe in different spots between measurements) and their average was used in the PLS model to ensure that possible sample inhomogeneities does not deteriorate the quantification.

Initially, a PLS model including only the unsieved ASA calibration samples was developed, when RMSEC and RMSECV of 0.54 and 1.21 % w/w were obtained, respectively, with the corresponding 0.998 and 0.992 R^2_C and R^2_{CV}. Although these values suggest a suitable calibration, testing the model on the at-line validation samples (*Valid C1, C3, C8, C10, C12, C14* from the continuous experiment) revealed that the model could not handle the effect of varying ASA particle size. Therefore, the model was modified by including the varying particle sizes of the calibration samples. This resulted in an RMSEC of 1.57, RMSECV of 1.88 % w/w, and R^2_C and R^2_{CV} of 0.978 and 0.969, respectively. Although these values indicate a worse model performance, this model was found to be

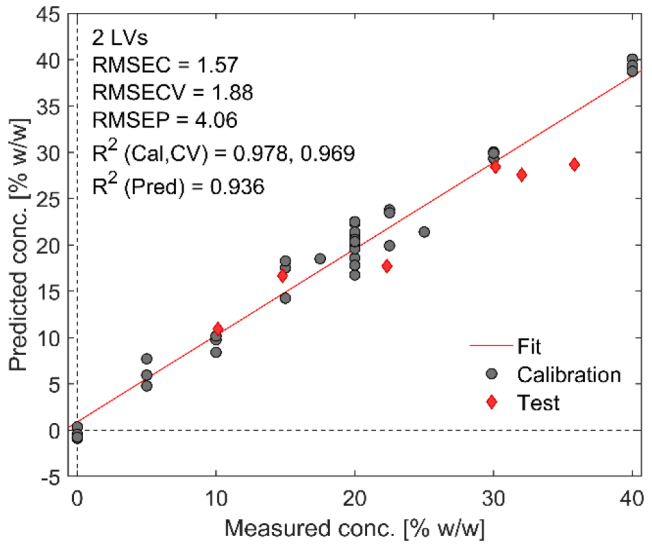

Fig. 5. PLS regression model for ASA content determination.

applicable to samples with different particle sizes. The PLS regression was built using the 8096–7984, 7170–7058, 6013–5785, and 4971–4859 cm^{-1} spectral ranges, which were determined by an automatic global optimization technique, namely the genetic algorithm variable selection algorithm. Notably, no spectral range was selected below 4850 cm^{-1}, where the most intensive particle size-dependent scattering was observed (see Fig. 4/b); therefore, it has the most detrimental effect on the ASA concentration determination.

The obtained calibration curve and the prediction of the six validation samples are depicted in Fig. 5. The RMSEP value (4.06 % w/w) derived from the six validation samples is considerably higher than the RMSEC and RMSECV. To understand this, it has to be accounted that the reference concentration values for the calibration samples (from which RMSEC and RMSECV are calculated) were determined by the accurate measurement of the blend components by analytical balance. In contrast, the reference for validation samples (for RMSEP calculation) was retrieved from the UV–VIS spectroscopic measurement at the 120 min dissolution time point. Consequently, the validation reference concentrations have an extra error component of the UV spectroscopic measurement. Furthermore, the NIR spectra of the validation samples were collected before encapsulation, while the reference concentration is determined from the capsule, which could result in further differences between the measured and predicted value, especially if slight inhomogeneities are present in the bulk powder sample from which 150 mg samples were taken during capsule filling. Furthermore, segregation or variation in the filling might also occur, *e.g.*, sticking of one of the components to the sample holder or spatula could result in differences between the NIR and UV spectroscopic measurements. Nevertheless, the model accuracy was deemed sufficient for the in-line, real-time monitoring application, especially accounting for these error factors in the validation measurements. However, further model improvement might be possible to apply as a validated, high-impact model for release testing.

The RMSEP value (4.06 % w/w) derived from the six validation samples is considerably higher than the RMSEC and RMSECV.

As concluded in Section 3.1, NIR spectra were found to carry the particle size information, which was the only critical factor affecting the *in vitro* dissolution of the capsules. Consequently, an ANN model was built as a surrogate for the dissolution measurement based on the NIR spectra. Although theoretically, a single ANN model could handle simultaneously the ASA concentration and the dissolution profile as outputs, we opted for developing a separate PLS regression for the concentration determination and an ANN for the dissolution rate as the

Table 2
Model goodness indicators of ANNs built by using different number of PCs.

Number of PCs used as input	f_1 (train)	f_2 (train)	f_1 (valid)	f_2 (valid)
2 PCs	1.19	88.3	2.24	80.5
3 PCs	1.09	89.7	2.26	80.1

qualitative analysis of the spectra showed that the utilization of different spectral ranges is advantageous for these tasks. The ANN was based on the entire spectral range preprocessed by SNV and first derivative. The dimension of the spectra was reduced before the ANN modeling by PCA, *i.e.*, the scores were used as the network inputs. The PCA model showed (see Section 3.1) that the first two PCs can be attributed to the ASA concentration and particle size changes, while PC 3 (1.2 % variance) could not be assigned to physical meaning. Consequently, ANN models were developed reducing the spectra dimension to two and three PCs. Consequently, this is a two-step approach, relying on a PCA model for dimension reduction followed by the ANN model. This is a general approach, which can drastically decrease the computational demand of the ANN modeling, as much fewer inputs (in this case two or three) are used compared to using the original spectral variables (in this work, 1213 variables). This results in the decrease of the trainable parameters (network weights, biases) by two magnitudes, which means faster training, better generalization of the model without considerable information loss.

The goodness indicators of the models in Table 2 show that using two or three PCs did not result in significantly different model performance: using 3 PCs moderately improved the training fit but provided an inferior prediction for the validation samples, suggesting an overfitting. Therefore, further in this work, the ANN model including two PCs is used.

The ANN model fitted well for all the training samples, irrespective of the ASA particle size or concentration. The lowest f_2 value of 71.8 was obtained for one of the samples including the 100–150 μm sieve fraction, and the highest f_2 value of 95.0 corresponded to a sample with the < 63 μm sieve fraction. Fitted and measured dissolution curves for selected training samples are illustrated in Fig. 6, and the measured and predicted dissolution curves of the six independent validation samples are included in Fig. 7. In Figs. 6 and 7, only the f_2 values are detailed for conciseness, as the f_1 and f_2 showed the same trends. Both the training and validation samples show good agreement between the calculated and measured curves, and the model could successfully distinguish between the fast and extended dissolution. It is also noticeable that, in general, the 95 % confidence limits (calculated by using bootstrap resampling as detailed in Section 2.4.4) of the fitted curves are narrow. Wider ranges can be seen for the 100–150 μm, 150–200 + 300–500 μm and 63–100 + 100–150 μm calibration samples, and for the *C10*, *C12*, *C14* validation samples. These are in the particle size region where the dissolution starts transitioning from fast dissolution to a more extended one. Therefore, the model confidence in this region could be further improved by including more samples with medium-sized drug particles.

3.3. Evaluation of the continuous blending experiment

The continuous blending experiment was conducted to demonstrate the in-line applicability of the ANN-based surrogate dissolution modeling in continuous pharmaceutical manufacturing for the first time. Such application can have great importance, especially in end-to-end continuous manufacturing lines, when changing raw material properties (*e.g.*, API particle size) must be identified in real-time and preferably compensated with appropriate control strategies. Furthermore, the method could be directly adapted for batch processes, *e.g.*, to monitor segregation problems during powder feeding in tableting.

To assess the suitability of the developed PLS and ANN model for the monitoring of the continuous blending process, the NIR spectra of the 19 samples (*C1-C19,* 'at-line samples') taken from the conveyor belt during

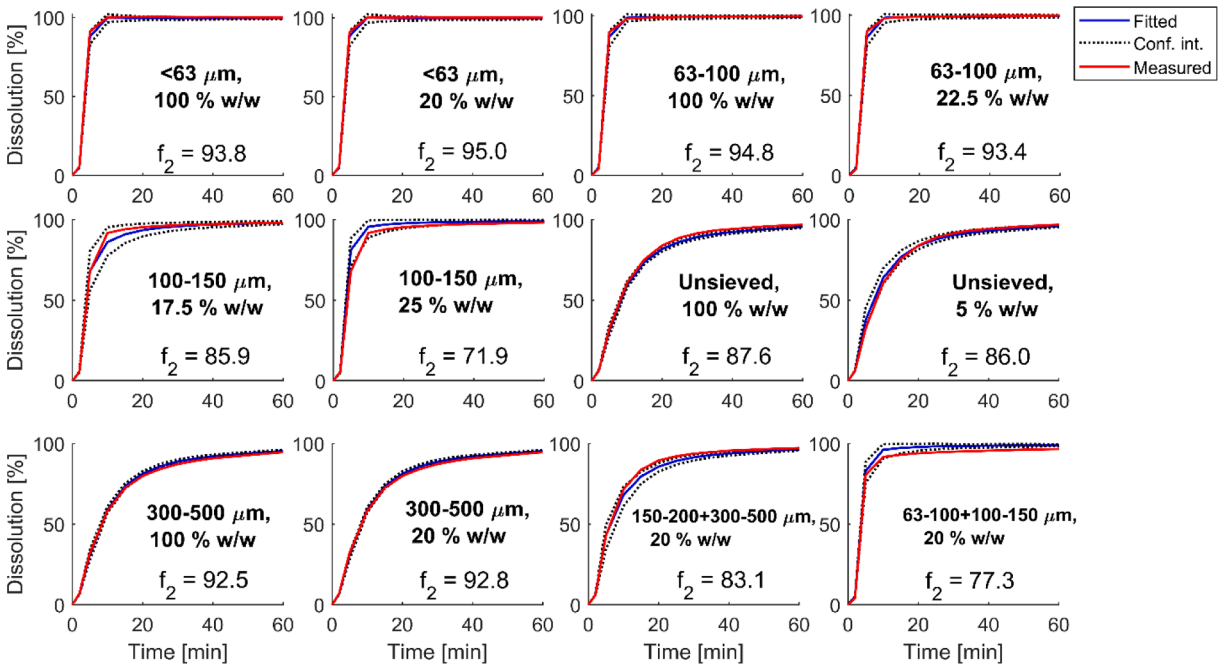

Fig. 6. Fitted and measured *in vitro* dissolution curves of selected training samples.

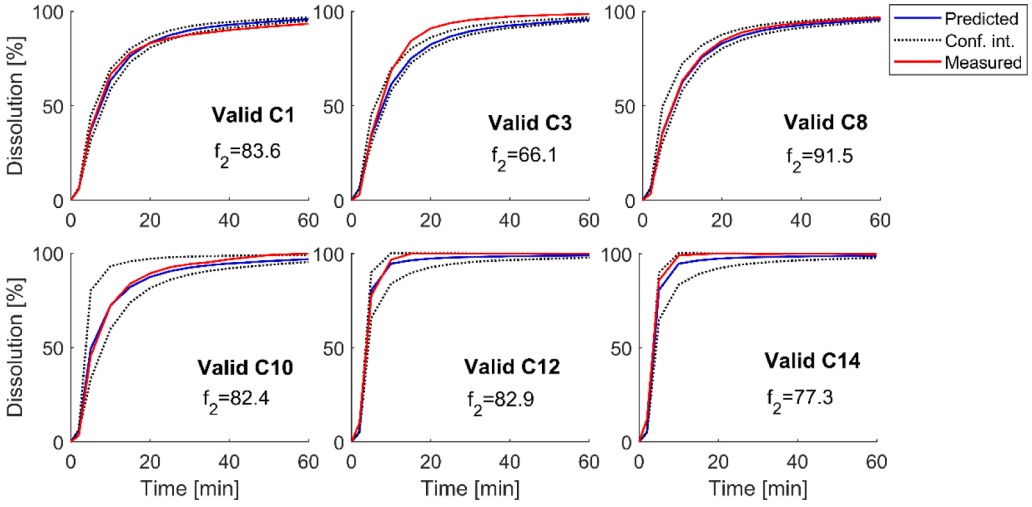

Fig. 7. Dissolution curves of the independent validation samples measured and predicted by NIR-based ANN.

the experiment as well as the in-line collected NIR spectra were analyzed.

First, the position of these samples within the PCA model space (Section 3.1.) was analyzed, which is illustrated for the at-line samples in Fig. 3. In Fig. 3, most at-line samples are grouped within the 150–200 μm particle size confidence ellipse. Based on the feed material during the experiment, these particles are expected to contain unsieved and 300–500 μm particles; *i.e.*, the NIR appears to identify them as smaller particle sizes. A few samples are separated from this group. *C5* corresponds to a sample with an expected 300–500 μm particle size, which is predicted by the PCA to have larger particles than that of the main group. *C1* and *C19* appear in the unsieved particle group but indicate lower drug concentration, which corresponds to the fact that these are from the start-up and shut-down phases of the experiment. The *C11-C13* samples originate from that experiment phase when the < 63 μm sieve fraction was fed as disturbance, which the PCA model correctly identifies as small particle size and low drug content. The in-line samples also showed a similar pattern, which is, however, not depicted in the score plot due to the large number of data points. These results confirm that the NIR spectroscopic monitoring, either at-line or in-line, could be used to monitor the general ASA content and particle size trends qualitatively and consequently identify out-of-specification manufacturing from the drug content and dissolution perspective.

The PLS regression model was applied on the at-line samples as well as on the in-line, real-time collected spectra. The predicted ASA concentrations are depicted in Fig. 8, along with the reference ASA concentration of the validation samples, which are extracted from the UV measurement of the dissolution testing of the 120 min dissolution time point. In Fig. 8, no significant difference was observed between the prediction of the at-line and in-line samples, and both showed excellent agreement with the UV reference concentration. Consequently, it could be concluded that the PLS model developed using only off-line calibration samples could reliably predict the drug concentration based on both at-line or in-line sample presentation.

The continuous blending was deliberately operated with initiating disturbances on the system to test the models' capability of identifying

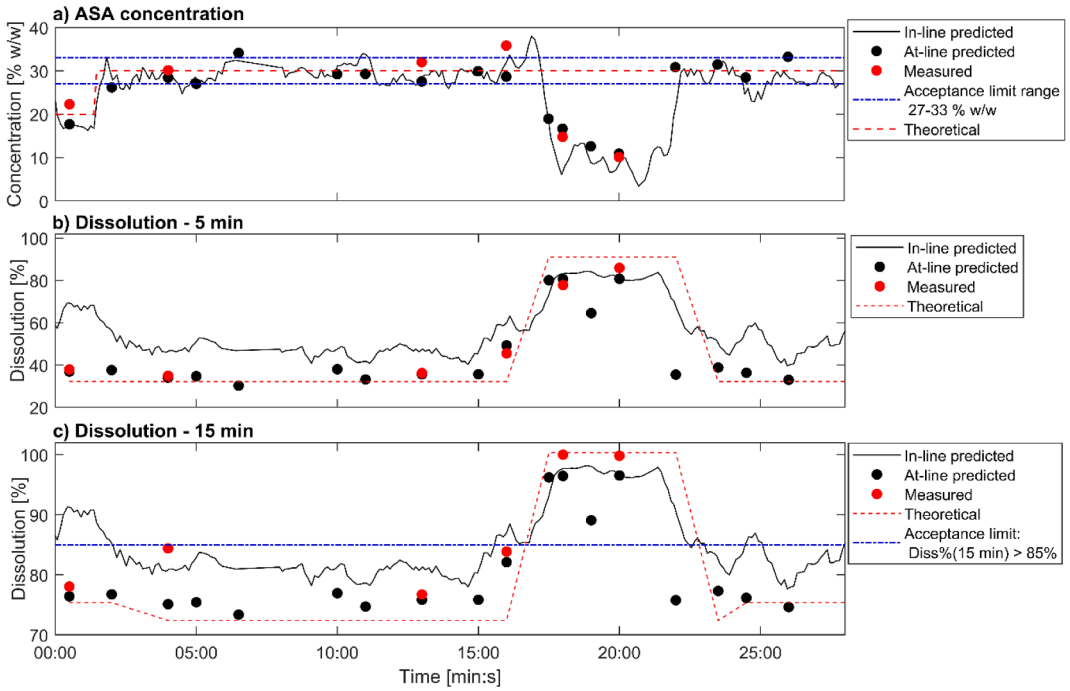

Fig. 8. Continuous blending experiment, monitoring of a) ASA concentration by the PLS regression model and dissolution % in the b) 5 min and c) 15 min dissolution timepoint by the ANN model. The 'in-line predicted' curves correspond to the values calculated from the in-line collected NIR spectra, the 'at-line predicted' points refer to the results of the C1-C19 at-line samples, the 'measured' points are the measurements of the UV spectroscopic reference method of the validation samples (Valid C1, C3, C8, C10, C12, C14) and the 'theoretical' curve refers to the expected value of the API content/ dissolution based on the experimental settings.

out-of-specification blends. The experiment was started by setting a 20 % w/w ASA content, which was then shifted to 30 % w/w at 2 min, which could be well monitored by the PLS model. After this, the 30 % w/w concentration could be kept constant with only a few measurement points outside the ± 10 % variation limit. The relative standard deviation was calculated to be 6.3 % between the 2 to 15 min time range (after 15 min, the process was deliberately disturbed, therefore, it is not accounted for in the calculation). Common acceptance criteria for the blend uniformity are that all individual results are within the ± 10 % variation limit, and the RSD is below 5 %. In this experiment, some measurement points were outside the ± 10 % variation limit, which caused the failing of the above-mentioned blend uniformity specification. Still, the model was capable to indicate non-conforming sections, which information could be further used for real-time diversion of the blend. The concentration drastically dropped to approximately 10 % w/w when the smallest (< 63 μm) sieve fraction was fed between 16 and 22 min. This shows the characteristics of volumetric feeding, *i.e.*, that the same feed rate of the smaller particle size results in a lower concentration in the blend. Furthermore, a worse powder flowability of the small sieve fraction also exacerbates this phenomenon. Nevertheless, the analysis of the continuous experiment demonstrated that the developed NIR-based PLS model could be applied for the blend uniformity analysis purposes, monitoring real-time if there are any potential issues caused by *e.g.*, segregation or inadequate feeding. The concentration fluctuations caused by the changing feedability of the powders could be eliminated by applying a spectroscopy-based feedback control, which has already been demonstrated in our previous studies [13,14]. Consequently, the model could not only be applied to monitor the blend uniformity but also to control it.

The full *in vitro* dissolution curves were calculated using the ANN model using both the at-line samples and the in-line collected spectra. In Fig. 8, only the dissolution values of the 5 and 15 min dissolution time points are depicted as the function of the experiment time. Furthermore, the 'theoretical' values in the figure indicate the expected values based on the measured dissolution values of the fed pure sieve fractions (< 63 μm, 300–500 μm, and unsieved) at the given time point. As already discussed, the results of the at-line validation samples (*Valid C1*, *C3*, *C8*, *C10*, *C12*, *C14*) showed excellent agreement with the measured dissolution curves (Fig. 7), as well as all the predictions made for the at-line samples correspond well with the theoretical values (Fig. 8/b, c) with the exception of a few outliers (such as the one around 18 min), which could be caused by either a sampling or NIR measurement error.

The predictions using the in-line collected spectra also followed the expected trends, *e.g.*, it could correctly indicate the faster dissolution caused by the feeding of small particles, although it provided less accurate predictions than the at-line approach with an offset between the in-line and at-line predictions. This could be caused by the fact that the NIR measurement is sensitive to environmental conditions, in which there is a significant difference when comparing the at-line and in-line setup, *e.g.*, stray light, sample thickness. For example, particle size determination by NIR spectroscopy has been previously found to be sensitive to sample presentation, *e.g.*, sample thickness [20] which can be critical during the continuous experiment, as the powder thickness on the conveyor belt was varied depending on the feed rate as well as the fed particle size. One approach to handle this would be to develop an in-line measurement setup where the variation of the powder amount is eliminated, *e.g.*, by measuring within a tableting feed frame or incorporating a sampling interface after the continuous blender that ensures a constant powder thickness. However, with the selection of the sampling place, the diversion strategy also needs to be accounted for, *i.e.*, if we want to divert the non-conforming material as a blend or only as a final dosage (after capsule filling or tableting). It is also important to note, that the calibration did not contain in-line spectra, which could also cause the off-set between the two measurement modes. The ANN model could also be further improved by including in-line collected spectra in the training set (although the powder thickness during the calibration spectra accumulation was not controlled).

Based on the presented results, it could be concluded that the NIR spectroscopy-based surrogate modeling was capable of determining the *in vitro* dissolution in a fast, non-destructive, and real-time manner. A

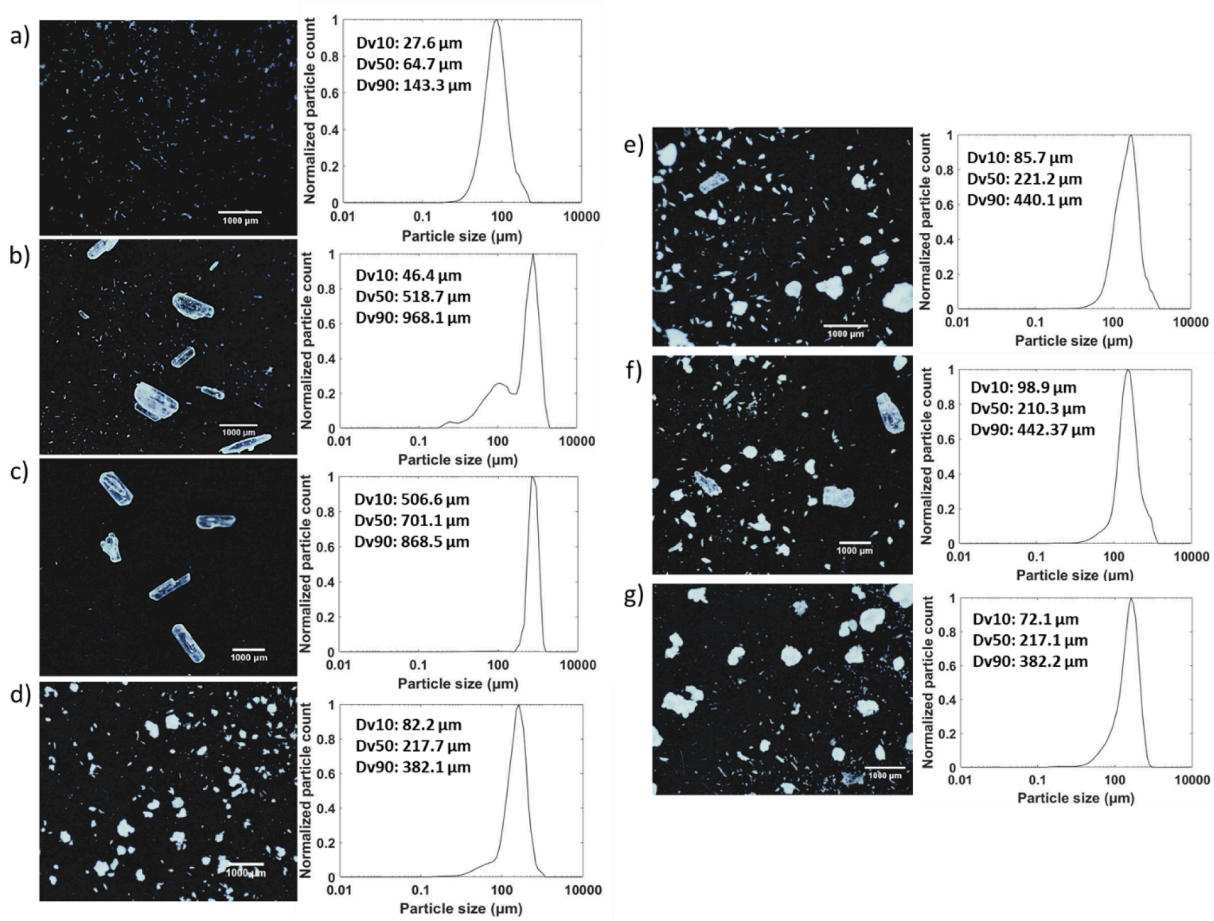

Fig. 9. The acquired, cropped images of the samples for the visualization of the particle sizes and the obtained particle size distributions from the acquired VIS images using machine vision (samples from the calibration set: a) ASA < 63 µm, b) ASA unsieved, c) ASA 300–500 µm, d) MCC; samples from the continuous experiment: e) C1, f) C10, g) C12).

possible acceptance limit for dissolution could be 85 % at 15 min, an often-used criterion for immediate-release formulations. It is visible in Fig. 8/c) that the at-line method could distinguish well if the capsule is below or above this level. The in-line measurement could also provide real-time information on the general trends during the process, with further possibilities for developing feedback control strategies based on the model. The at-line measurement could also be a viable and advantageous approach, *e.g.,* for stratified sampling strategies, and its accuracy might be suitable for a validated surrogate model. In this case, the lengthy dissolution testing could be replaced by a few seconds long, non-destructive NIR measurement next to the continuous manufacturing line.

3.4. Machine vision-based particle size analysis

As demonstrated in the previous sections, the NIR spectra carry information simultaneously on the constitution of the blends and particle size. However, particle size information manifests as subtle spectral changes sensitive to environmental factors. Therefore, a direct particle size measurement technique was performed on the sample to validate the NIR models. Instead of the conventional PSD measurement approaches, such as laser diffraction, a machine vision-based particle size analysis was used, which is an emerging, non-destructive technique. The applied method is similar to a microscopic particle size determination; however, it offers high-resolution images, easy accessibility and cost-effectiveness.

VIS images were used to evaluate the particle size of the different ASA sieve fractions, MCC, and powder blends. Fig. 9 summarizes the acquired images and the obtained PSDs. The acquired images of the samples exhibit similarities to microscopic measurements, but due to its portable and affordable nature, as well as its rapidity, it could be used as a PAT tool.

Differences in the pure ASA samples (Fig. 9/a, b, c) are visible on the images and the obtained PSD and statistical parameters. In the case of the unsieved sample (Fig. 9/b) there is a great variation in particle sizes compared to the sieved groups. The PSD of the applied excipient was also found to be in the same range as the unsieved ASA, which can potentially complicate the machine vision-based analysis of the blends, especially with lower ASA content. Furthermore, measuring powder blends where both the API and excipient are visible in the images poses a challenge, especially when dealing with broad particle size ranges. In the case of large particles (> 500 µm), the image processing algorithm can remove agglomerates, but in certain scenarios, the ASA particle was found to form aggregates with the MCC particles, leading to its exclusion from the measurement. As for the small particles (< 63 µm), accurately quantifying them due to the low resolution can be challenging even with artificial intelligence-based image processing. Nonetheless, the obtained images could provide insight into the presence of both small and large particles in the system and were suitable for assessing the variations among the samples.

The *C1-C11* and *C15-C19* continuous experiment samples showed the presence of larger API particles due to the feeding of the unsieved and the 300–500 µm ASA. This was also reflected in the slight variation of Dv10 and Dv90 values among the groups, which is shown in Fig. 9 for *C1* and *C10*. The images obtained from the *C12-C14* samples did not show large API particles, which is attributed to introducing the < 63 µm

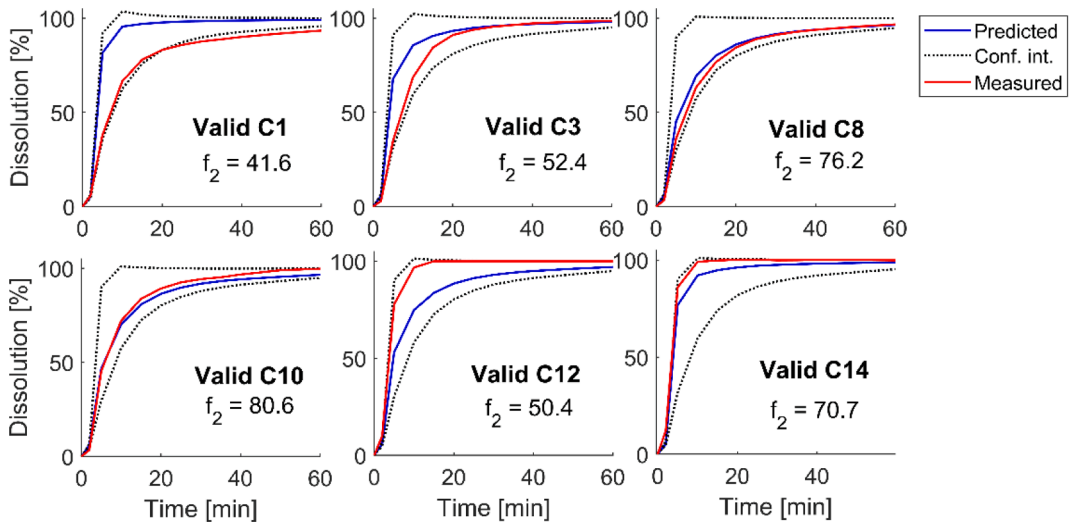

Fig. 10. Dissolution curves of the independent validation samples measured and predicted by machine vision-based ANN.

group into the system (in Fig. 9, C12 is illustrated). These observations correspond with the measured and predicted *in vitro* dissolution curves, further validating the NIR modeling results.

The utilization of the derived PSD curves was also assessed as a means of quantifying the dissolution curve by an ANN model. In this case, the PSD represented as the Dv10, Dv50, Dv90, D10, D32, and D43 statistical parameters were used as the model input, together with the ASA content derived from the PLS model. The ANN model provided a mean f_2 of 88.7 and mean f_1 of 1.11 for training sample set, which is comparable with the NIR-based model, but the validation yielded significantly lower model performance with mean f_2 of 62.0 and mean f_1 of 5.25 and wider confidence intervals (see Fig. 10). Although this suggests that further refinement of the derived PSD data or more training samples would be beneficial, the potential of the machine vision-based dissolution surrogate model is demonstrated.

These findings indicate the validity of the NIR-based modeling, relying on an indirect PSD characterization as opposed to the direct PSD measurement by the imaging system. The machine vision could be applied at-line as a non-destructive technique, which enables a comprehensive understanding of the blends produced in the continuous operations by the visual distinction. Seeing the potential of the machine vision-based dissolution modeling, future work will address the in-line implementation of the machine vision-based dissolution prediction. This could require the development of special sampling interface to integrate the system into the continuous manufacturing setup, the enhancement of the camera configuration and background selection. Furthermore, is would be also necessary to address the handling of both the agglomerates and fines, for which the integration of deep neural networks would be necessary.

4. Conclusions

This work presented the first application of an ANN-based real-time surrogate modeling of *in vitro* dissolution coupled with in-line blend uniformity measurement. It was possible to obtain the blend concentration and the full *in vitro* dissolution curve in real-time based on in-line and at-line collected NIR spectra. The machine vision-based PSD evaluation supported the obtained results, the images giving similar information to microscopic measurements but in a way that meets the requirement of PAT, *i.e.*, a rapid, non-destructive, and cost-effective measurement. The models were deliberately tested by feeding different particle fractions, provoking out-of-specification samples. The blend uniformity problems experienced when the < 63 μm particle fraction was fed could be eliminated by applying a concentration-based feedback control [13]. However, the characterization of particle size-dependent dissolution still remains essential, for example, in end-to-end manufacturing lines, when the quality of the incoming raw material might vary (*e.g.*, due to the preceding crystallization step) or when there is a risk for segregation. Future studies will aim to develop control strategies, implement an in-line machine vision measurement layout, and utilize advanced segmentation methods for in-line applications. Furthermore, in-line applied dissolution models involving multiple CMAs and CPPs could also be tested.

The results showed that the in-line determination of the dissolution by surrogate models could be used in a control strategy or automatically isolate out-of-specification product sections during the continuous process. Nevertheless, in the case of applying the models for RTRT, the high impact of the models also must be taken into consideration [29], meaning that further validation is needed, establishing, *e.g.*, proper strategy for stratified sampling, maintenance, and acceptance criteria.

CRediT authorship contribution statement

Lilla Alexandra Mészáros: Writing – original draft, Visualization, Software, Methodology, Investigation. **Martin Gyürkés:** Visualization, Software, Investigation. **Emese Varga:** Investigation. **Kornélia Tacsi:** Investigation. **Barbara Honti:** Writing – review & editing, Investigation. **Enikő Borbás:** Writing – review & editing. **Attila Farkas:** Writing – review & editing, Software. **Zsombor Kristóf Nagy:** Writing – review & editing, Funding acquisition, Conceptualization. **Brigitta Nagy:** Writing – original draft, Visualization, Software, Methodology, Funding acquisition, Conceptualization.

Data availability

Data will be made available on request.

Acknowledgments

The research reported in this paper and carried out at BME has been supported by the National Laboratory of Artificial Intelligence, funded by the NRDIO under the auspices of the Ministry for Innovation and Technology. Supported by the OTKA grant PD 142970, ÚNKP-23-5-BME-443 and ÚNKP-23-4-I-BME-257 New National Excellence Program of the Ministry for Culture and Innovation from the Source of the National Research, Development and Innovation Fund. The research was also supported by the János Bolyai Research Scholarship of the Hungarian Academy of Sciences. Part of the work is supported by project

2020-1.1.2-PIACI-KFI-2021-00218.

References

[1] C. Badman, C.L. Cooney, A. Florence, K. Konstantinov, M. Krumme, S. Mascia, M. Nasr, B.L. Trout, Why We Need Continuous Pharmaceutical Manufacturing and How to Make It Happen, J. Pharm. Sci. 108 (2019) 3521–3523, https://doi.org/10.1016/j.xphs.2019.07.016.

[2] A. Domokos, B. Nagy, B. Szilágyi, G. Marosi, Z.K. Nagy, Integrated Continuous Pharmaceutical Technologies - A Review, Org. Process Res. Dev. 25 (2021), https://doi.org/10.1021/acs.oprd.0c00504.

[3] Food and Drug Administration, 2004. Guidance for industry, PAT-A framework for innovative pharmaceutical development, manufacturing and quality assurance.

[4] European Medical Agency, 2012. Guideline on real time release testing (formerly Guideline on parametric release).

[5] ICH, 2023. ICH guideline Q13 on continuous manufacturing of drug substances and drug products - Scientific guideline.

[6] E.-A. Jung, Y.-J. Park, J.-E. Kim, Application of continuous manufacturing for solid oral dosage forms, J. Pharm. Investig. 53 (2023) 457–474, https://doi.org/10.1007/s40005-023-00619-w.

[7] D. Markl, M. Warman, M. Dumarey, E.-L. Bergman, S. Folestad, Z. Shi, L.F. Manley, D.J. Goodwin, J.A. Zeitler, Review of real-time release testing of pharmaceutical tablets: State-of-the art, challenges and future perspective, Int. J. Pharm. 582 (2020) 119353, https://doi.org/10.1016/j.ijpharm.2020.119353.

[8] N.L. Velez, J.K. Drennen, C.A. Anderson, Challenges, opportunities and recent advances in near infrared spectroscopy applications for monitoring blend uniformity in the continuous manufacturing of solid oral dosage forms, Int. J. Pharm. 615 (2022) 121462, https://doi.org/10.1016/J.IJPHARM.2022.121462.

[9] N.O. Sierra-Vega, A. Román-Ospino, J. Scicolone, F.J. Muzzio, R.J. Romañach, R. Méndez, Assessment of blend uniformity in a continuous tablet manufacturing process, Int. J. Pharm. 560 (2019) 322–333, https://doi.org/10.1016/J.IJPHARM.2019.01.073.

[10] A.P. Karttunen, J. Poms, S. Sacher, A. Sparén, C. Ruiz Samblás, M. Fransson, L. Martin De Juan, J. Remmelgas, H. Wikström, W.K. Hsiao, S. Folestad, O. Korhonen, S. Abrahmsén-Alami, P. Tajarobi, Robustness of a continuous direct compression line against disturbances in feeding, Int. J. Pharm. 574 (2020) 118882, https://doi.org/10.1016/J.IJPHARM.2019.118882.

[11] J. Palmer, C.J. O'Malley, M.J. Wade, E.B. Martin, T. Page, G.A. Montague, Opportunities for Process Control and Quality Assurance Using Online NIR Analysis to a Continuous Wet Granulation Tableting Line, J. Pharm. Innov. 15 (2020) 26–40, https://doi.org/10.1007/s12247-018-9364-7.

[12] M. Gyürkés, L. Madarász, Á. Köte, A. Domokos, D. Mészáros, Á.K. Beke, B. Nagy, G. Marosi, H. Pataki, Z.K. Nagy, A. Farkas, Process design of continuous powder blending using residence time distribution and feeding models, Pharmaceutics 12 (2020), https://doi.org/10.3390/pharmaceutics12111119.

[13] M. Gyürkés, K. Tacsi, H. Pataki, A. Farkas, Residence Time Distribution-Based Smith Predictor: an Advanced Feedback Control for Dead Time-Dominated Continuous Powder Blending Process, J. Pharm. Innov. 18 (2023) 1381–1394, https://doi.org/10.1007/s12247-023-09728-3.

[14] B. Nagy, A. Farkas, M. Gyürkés, S. Komaromy-Hiller, B. Démuth, B. Szabó, D. Nusser, E. Borbás, G. Marosi, Z.K. Nagy, In-line Raman spectroscopic monitoring and feedback control of a continuous twin-screw pharmaceutical powder blending and tableting process, Int. J. Pharm. 530 (2017), https://doi.org/10.1016/j.ijpharm.2017.07.041.

[15] D.L. Galata, L.A. Mészáros, M. Ficzere, P. Vass, B. Nagy, E. Szabó, A. Domokos, A. Farkas, I. Csontos, G. Marosi, Z.K. Nagy, Continuous blending monitored and feedback controlled by machine vision-based PAT tool, J. Pharm. Biomed. Anal. 196 (2021) 113902, https://doi.org/10.1016/j.jpba.2021.113902.

[16] T.R. Hörmann-Kincses, M. Beretta, J. Kruisz, F. Stauffer, G. Birk, P.M. Piccione, J. Holman, J.G. Khinast, Predicting powder feedability: A workflow for assessing the risk of flow stagnation and defining the operating space for different powder-feeder combinations, Int. J. Pharm. 629 (2022) 122364, https://doi.org/10.1016/J.IJPHARM.2022.122364.

[17] Jakubowska, E., Ciepluch, N., 2021. Blend Segregation in Tablets Manufacturing and Its Effect on Drug Content Uniformity—A Review. Pharmaceutics 2021, Vol. 13, Page 1909 13, 1909. 10.3390/PHARMACEUTICS13111909.

[18] M. Jaspers, M.T.W. de Wit, S.S. Kulkarni, B. Meir, P.H.M. Janssen, M.M.W. van Haandel, B.H.J. Dickhoff, Impact of excipients on batch and continuous powder blending, Powder Technol. 384 (2021) 195–199, https://doi.org/10.1016/J.POWTEC.2021.02.014.

[19] D.R. Ely, M. Thommes, M.T. Carvajal, Analysis of the effects of particle size and densification on NIR spectra, Colloids Surf A Physicochem Eng Asp 331 (2008) 63–67, https://doi.org/10.1016/J.COLSURFA.2008.07.017.

[20] M.C. Pasikatan, J.L. Steele, C.K. Spillman, E. Haque, Near Infrared Reflectance Spectroscopy for Online Particle Size Analysis of Powders and Ground Materials, J. Near Infrared Spectrosc. 9 (2001) 153–164.

[21] M. Razuc, A. Grafia, L. Gallo, M.V. Ramírez-Rigo, R.J. Romañach, Near-infrared spectroscopic applications in pharmaceutical particle technology, Drug Dev. Ind. Pharm. 45 (2019) 1565–1589, https://doi.org/10.1080/03639045.2019.1641510.

[22] M.J. Barajas, A.R. Cassiani, W. Vargas, C. Conde, J. Ropero, J. Figueroa, R. J. Romañach, Near-Infrared Spectroscopic Method for Real-Time Monitoring of Pharmaceutical Powders during Voiding, Appl. Spectrosc. 61 (2007) 490–496, https://doi.org/10.1366/000370207780807713.

[23] D.L. Galata, L.A. Mészáros, N. Kállai-Szabó, E. Szabó, H. Pataki, G. Marosi, Z. K. Nagy, Applications of machine vision in pharmaceutical technology: A review, Eur. J. Pharm. Sci. 159 (2021) 105717, https://doi.org/10.1016/j.ejps.2021.105717.

[24] A.F.T. Silva, A. Burggraeve, Q. Denon, P. Van der Meeren, N. Sandler, T. Van Den Kerkhof, M. Hellings, C. Vervaet, J.P. Remon, J.A. Lopes, T. De Beer, Particle sizing measurements in pharmaceutical applications: Comparison of in-process methods versus off-line methods, Eur. J. Pharm. Biopharm. 85 (2013) 1006–1018, https://doi.org/10.1016/j.ejpb.2013.03.032.

[25] M. Javaid, A. Haleem, R.P. Singh, S. Rab, R. Suman, Exploring impact and features of machine vision for progressive industry 4.0 culture, Sensors International 3 (2022) 100132, https://doi.org/10.1016/J.SINTL.2021.100132.

[26] M. Ficzere, O. Péterfi, A. Farkas, Z.K. Nagy, D.L. Galata, Image-based simultaneous particle size distribution and concentration measurement of powder blend components with deep learning and machine vision, Eur. J. Pharm. Sci. 191 (2023) 106611, https://doi.org/10.1016/J.EJPS.2023.106611.

[27] L. Madarász, L.A. Mészáros, Á. Köte, A. Farkas, Z.K. Nagy, AI-based analysis of in-line process endoscope images for real-time particle size measurement in a continuous pharmaceutical milling process, Int. J. Pharm. 641 (2023) 123060, https://doi.org/10.1016/J.IJPHARM.2023.123060.

[28] A.S. Sousa, J. Serra, C. Estevens, R. Costa, A.J. Ribeiro, A quality by design approach in oral extended release drug delivery systems: where we are and where we are going? J. Pharm. Investig. 53 (2023) 269–306, https://doi.org/10.1007/s40005-022-00603-w.

[29] M. Kakhi, J. Li, A. Dorantes, Regulatory Experience with Continuous Manufacturing and Real Time Release Testing for Dissolution in New Drug Applications, J. Pharm. Sci. 112 (2023) 2604–2614, https://doi.org/10.1016/j.xphs.2023.08.004.

[30] B. Nagy, D. Petra, D.L. Galata, B. Démuth, E. Borbás, G. Marosi, Z.K. Nagy, A. Farkas, Application of artificial neural networks for Process Analytical Technology-based dissolution testing, Int. J. Pharm. 567 (2019), https://doi.org/10.1016/j.ijpharm.2019.118464.

[31] K. Ojala, M. Myrskyranta, A. Liimatainen, H. Kortejärvi, A. Juppo, Prediction of drug dissolution from Toremifene 80 mg tablets by NIR spectroscopy, Int. J. Pharm. 577 (2020) 119028, https://doi.org/10.1016/J.IJPHARM.2020.119028.

[32] P. Pawar, Y. Wang, G. Keyvan, G. Callegari, A. Cuitino, F. Muzzio, Enabling real time release testing by NIR prediction of dissolution of tablets made by continuous direct compression (CDC), Int. J. Pharm. 512 (2016) 96–107, https://doi.org/10.1016/j.ijpharm.2016.08.033.

[33] Zhao, Y., Li, W., Shi, Z., Drennen, J.K., Anderson, C.A., 2019. Prediction of Dissolution Profiles from Process Parameters, Formulation and Spectroscopic Measurements. J Pharm Sci. 10.1016/j.xphs.2019.01.023.

[34] D.L. Galata, B. Zsiros, L.A. Mészáros, B. Nagy, E. Szabó, A. Farkas, Z.K. Nagy, Raman mapping-based non-destructive dissolution prediction of sustained-release tablets, J. Pharm. Biomed. Anal. 212 (2022), https://doi.org/10.1016/j.jpba.2022.114661.

[35] K. Matsunami, T. Miura, K. Yaginuma, S. Tanabe, S. Badr, H. Sugiyama, Surrogate modeling of dissolution behavior toward efficient design of tablet manufacturing processes, Comput. Chem. Eng. 171 (2023) 108141, https://doi.org/10.1016/j.compchemeng.2023.108141.

[36] B. Nagy, B. Szilágyi, A. Domokos, B. Vészi, K. Tacsi, Z. Rapi, H. Pataki, G. Marosi, Z. K. Nagy, Z.K. Nagy, Dynamic flowsheet model development and digital design of continuous pharmaceutical manufacturing with dissolution modeling of the final product, Chem. Eng. J. 419 (2021) 129947, https://doi.org/10.1016/j.cej.2021.129947.

[37] C. Gendre, M. Boiret, M. Genty, P. Chaminade, J.M. Pean, Real-time predictions of drug release and end point detection of a coating operation by in-line near infrared measurements, Int. J. Pharm. 421 (2011) 237–243, https://doi.org/10.1016/J.IJPHARM.2011.09.036.

[38] Q. Su, P. Hermant, F. Casati, B. Halkude, W. Wu, A. Ramnath, A. Dubey, S. Born, B. Takizawa, S. Mascia, Model predictive in vitro dissolution testing in pharmaceutical continuous manufacturing: An equivalence study, AIChE J 69 (2023) e18124.

[39] A. Domokos, B. Nagy, M. Gyürkés, A. Farkas, K. Tacsi, H. Pataki, Y.C. Liu, A. Balogh, P. Firth, B. Szilágyi, G. Marosi, Z.K. Nagy, Z.K. Nagy, End-to-end continuous manufacturing of conventional compressed tablets: From flow synthesis to tableting through integrated crystallization and filtration, Int. J. Pharm. 581 (2020) 119297, https://doi.org/10.1016/j.ijpharm.2020.119297.

[40] K. Tacsi, H. Pataki, A. Domokos, B. Nagy, I. Csontos, I. Markovits, F. Farkas, Z. K. Nagy, G. Marosi, Direct Processing of a Flow Reaction Mixture Using Continuous Mixed Suspension Mixed Product Removal Crystallizer, Cryst. Growth Des. 20 (2020) 4433–4442, https://doi.org/10.1021/acs.cgd.0c00252.

[41] L.A. Mészáros, D.L. Galata, L. Madarász, Á. Köte, K. Csorba, Á.Z. Dávid, A. Domokos, E. Szabó, B. Nagy, G. Marosi, A. Farkas, Z.K. Nagy, Digital UV/VIS imaging: A rapid PAT tool for crushing strength, drug content and particle size distribution determination in tablets, Int. J. Pharm. 578 (2020) 119174.

[42] Food and Drug Administration, 2018. Guidence for Industry. Dissolution Testing and Acceptance Criteria for Immediate-Release Solid Oral Dosage Form Drug Products Containing High Solubility Drug Substances.

[43] P. Costa, J.M. Sousa Lobo, Modeling and comparison of dissolution profiles, Eur. J. Pharm. Sci. 13 (2001) 123–133, https://doi.org/10.1016/S0928-0987(01)00095-1.

[44] Food and Drug Administration, 1997. Guidance for Industry. Dissolution Testing of Immediate Release Solid Oral Dosage Forms.